IEEE Photonics Journal
An IEEE Photonics Society Publication

Open Access

Etched Silicon-on-Insulator Microring Resonator for Ultrasound Measurement

Volume 12, Number 2, April 2020

Wenjian Yang
Shijie Song
Keith Powell
Xiaoyi Tian
Liwei Li
Linh Nguyen
Xiaoke Yi

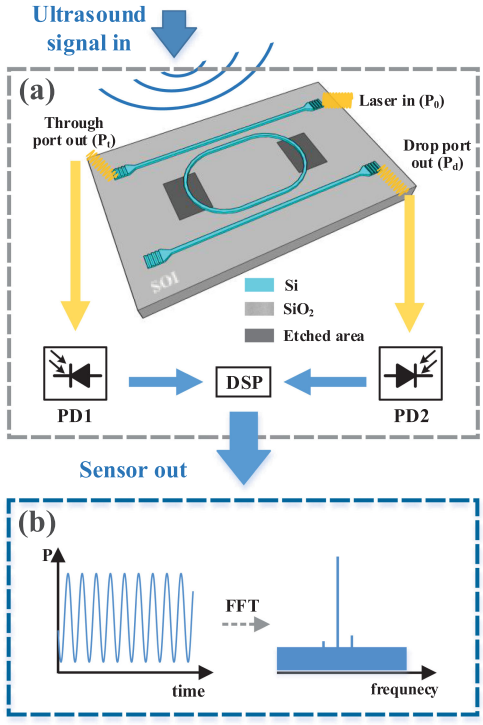

DOI: 10.1109/JPHOT.2020.2978947

Etched Silicon-on-Insulator Microring Resonator for Ultrasound Measurement

Wenjian Yang, Shijie Song, Keith Powell, Xiaoyi Tian, Liwei Li, Linh Nguyen, and Xiaoke Yi

School of Electrical and Information Engineering, Faculty of Engineering and Information Technologies, The University of Sydney, Camperdown, NSW 2006, Australia

DOI:10.1109/JPHOT.2020.2978947

Manuscript received December 20, 2019; revised January 18, 2020; accepted February 29, 2020. Date of publication March 6, 2020; date of current version April 14, 2020. This work was supported in part by Australian Research Council and in part by the Harvard University Mobility Scheme. Corresponding author: Xiaoke Yi (e-mail: xiaoke.yi@sydney.edu.au).

Abstract: A novel integrated optical ultrasound sensor based on silicon-on-insulator (SOI) platform is proposed, theoretically analyzed and experimentally demonstrated. By using a selectively etched SOI microring resonator in an add-drop structure, the technique provides a linear and distortion-free sensing response to the ultrasound signal as it prevents the coupling region deformation and removes variations from the power fluctuation of the optical source. The proof-of-concept experimental demonstration of the proposed sensor shows the detection of air-coupled ultrasound pressure at different frequencies and magnitudes, a frequency sensing resolution of 30 Hz and a wide acceptance angle around 75 degrees.

Index Terms: Optical sensors, optical resonators, photonic integrated circuits, integrated optics devices.

1. Introduction

Utrasound sensor devices, which allow detection and imaging using acoustic waves, have found many applications in biomedical imaging, object recognition and structural health monitoring [1]–[4]. The photonic based detection method provides superior advantages over conventional piezoelectric technology with distinct features including strong immunity to electromagnetic interference, high durability and reduced weight and footprint [5], [6]. Fiber-optic approaches such as fiber-optic interferometers, microbend fiber sensors and fiber Bragg gratings have been proposed to achieve ultrasound detection in recent decade [7]–[10]. Integrated photonic sensors have garnered much interest recently due to its small size, mass producibility and low cost. A Mach-Zehnder interferometer (MZI) ultrasound sensor with one sensing arm located on a membrane of size 121 μm by 121 μm is presented in [11]. It has a moderate spectrum transmission slope which limits the potential to achieve a highly sensitive ultrasound sensor. Optical resonators which feature high sensitivity with more compact size due to their inherent resonance effect bring key benefits to photonic sensing. Different ultrasound detectors using optical resonators have been proposed [4], [12]–[15]. In [4], the usage of spoked silica microdisk requires evanescently coupled into, and out of, the microdisk via an optical nanofiber which limits the capability of scaling up the structure to large sensor arrays. Polymer waveguides [12], [13] and silicon-on-insulator (SOI) waveguides on membrane [14], [15] based ultrasound sensors have been presented by using an all-pass configuration where a ring waveguide is coupled to a straight bus waveguide. The resonance shifting of ring resonators is

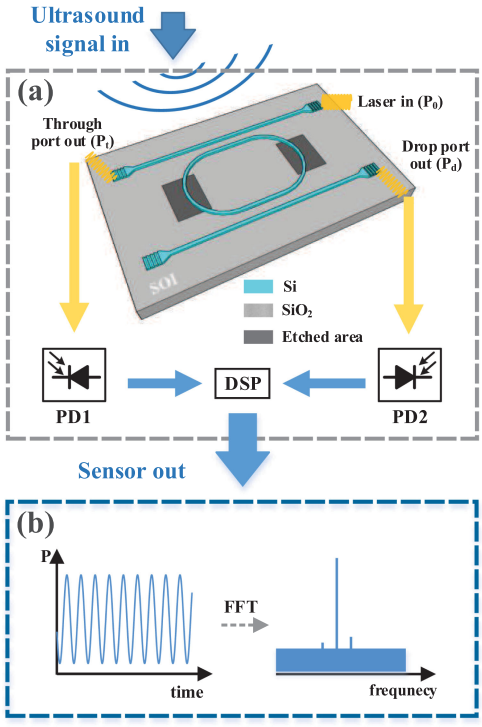

Fig. 1. (a) Schematic diagram of the proposed ultrasound sensor system. (b) Sketch of the expected ultrasound measurement output. FFT: fast Fourier transform.

monitored by detecting the optical power at the edge of the microring notch filter [13]–[15]. In these structures, the coupling region between the bus waveguide and ring waveguide is sensitive to the incident acoustical pressure waves, which affects the transmitted optical power to the resonators and induces unwanted notch depth variations that will degrade the sensing performance. Moreover, the optical power detection approach by placing a laser at one side of the transmission spectrum suffers from power fluctuation of the optical source.

In this paper, we propose and demonstrate a new ultrasound sensor based on a selectively etched add-drop microring resonator structure to provide a linear and distortion-free response to the ultrasound signal by preventing the coupling region deformation and removing variations from the power fluctuation of the optical source. This is achieved via selectively etching the targeted region of the silicon microring to enhance the ultrasound-induced mechanical deformation while the coupling regions remain unetched to ensure the coupling coefficient of the sensor is ultrasound insensitive. By using both through and drop ports of the add-drop microring for signal processing, we obtain the transfer function between the applied ultrasound signal and the sensor output which has a linear relationship with the applied strain. As a proof of concept, we demonstrate an ultrasound sensor fabricated through the CMOS-compatible SOI platform experimentally showing the detection of air-coupled ultrasound pressure of 4 Pa, a frequency sensing resolution of 30 Hz and a wide acceptance angle around 75 degrees.

2. Principle of Operation

Fig. 1(a) illustrates the schematic diagram of the proposed ultrasound sensor system which contains an add-drop SOI microring resonator, a single wavelength laser source, photodetectors and a digital signal processing (DSP) unit. When ultrasound pressure waves are applied on the microring resonator, it generates a deformation on the silicon waveguide which is expressed

as [16], [17]

$$\epsilon(t) = \frac{-(1+\nu)(1-2\nu)P(t)}{E} \tag{1}$$

where $\epsilon(t)$ is the time-varying strain, ν is Poisson's ratio, E is Young's modulus and $P(t)$ is the applied ultrasound pressure, which decreases with the increasing distance between the ultrasound source and the sensor probe [18]. The ultrasound-induced strain affects the optical resonance in two ways: the strain-induced elongation of resonator circumference and the effective refractive index change. The combination of both effects contributes to the strain-induced resonant wavelength shift (λ_m) of the microring resonator given by [19], [20]

$$\frac{d\lambda_m}{d\epsilon} = \frac{\lambda}{n_g}\left(n_e + \frac{dn_e}{d\epsilon}\right) \tag{2}$$

where λ is the resonance wavelength when no ultrasound is applied, n_g and n_e are the group index and the effective refractive index of the waveguide respectively, and $dn_e/d\epsilon$ is the strain-induced effective index change.

When the laser light is injected into the add-drop microring resonator with the wavelength fixed at the edge of the optical resonance curve, this ultrasound-induced resonant wavelength shift directly translates into the modulation of the light intensity. The transmitted optical power Pt and the drop port power Pd of the add-drop microring resonator are given by

$$P_t = P_0 \frac{r^2(1-a)^2 + 4ar^2\sin^2\left(\frac{\pi\Delta\lambda}{FSR}\right)}{(1-ar^2)^2 + 4ar^2\sin^2\left(\frac{\pi\Delta\lambda}{FSR}\right)} \tag{3}$$

$$P_d = P_0 \frac{k^4 a}{(1-ar^2)^2 + 4ar^2\sin^2\left(\frac{\pi\Delta\lambda}{FSR}\right)} \tag{4}$$

where P_0 is the incident laser power, a is the round-trip amplitude transmission, r is the field self-coupling coefficient, k is the field cross-coupling coefficient, $\Delta\lambda$ is the ultrasound induced wavelength change and FSR is the free spectral range which in practice is much larger than the resonance wavelength shift, i.e. $FSR \gg \Delta\lambda$.

We use optical photodetectors to map optical power change to electrical domain. Considering that the high refractive index contrast of the SOI waveguide allows a negligible round-trip attenuation for the proposed microring resonator [21], i.e. $a \approx 1$, the strain-induced variations of the photocurrents for the through and the drop ports after photodetection can be expressed as

$$\frac{dI_t}{d\epsilon} = \frac{dP_t}{d\epsilon}\cdot R_t = \frac{4P_0R_tr^2[\pi L_0(1+\epsilon(t))(n_e+\frac{dn_e}{d\epsilon})]^2}{(1-r^2)^2\lambda + 4r^2[\pi L_0(1+\epsilon(t))(n_e+\frac{dn_e}{d\epsilon})]^2} \tag{5}$$

$$\frac{dI_d}{d\epsilon} = \frac{dP_d}{d\epsilon}\cdot R_d = \frac{P_0R_dk^4}{(1-r^2)^2\lambda + 4r^2[\pi L_0(1+\epsilon(t))(n_e+\frac{dn_e}{d\epsilon})]^2} \tag{6}$$

where L_0 is the circumference of the microring resonator, R_t and R_d are the responsivities of the photodetectors after each optical output port, respectively.

We define the square root of the ratio of the strain-induced photocurrents variations at the through port to the drop port as the sensor system transfer function, which is given by

$$h(t) = \frac{2\pi r}{1-r^2}\sqrt{\frac{R_t}{R_d}}\cdot\frac{L_0(1+\epsilon(t))}{\lambda}\left(n_e + \frac{dn_e}{d\epsilon}\right) \tag{7}$$

The derived transfer function is a general form for either etched or non-etched microring resonator. It has has a linear relationship with the applied strain $\epsilon(t)$, as the strain-induced effective index change ($dn_e/d\epsilon$) can be neglected for silicon waveguides with a constant waveguide width [20]. Since the transfer function is not related to the input laser power (P_0), the influence of the power fluctuation of the optical source on the sensor performance can be completely eliminated. The

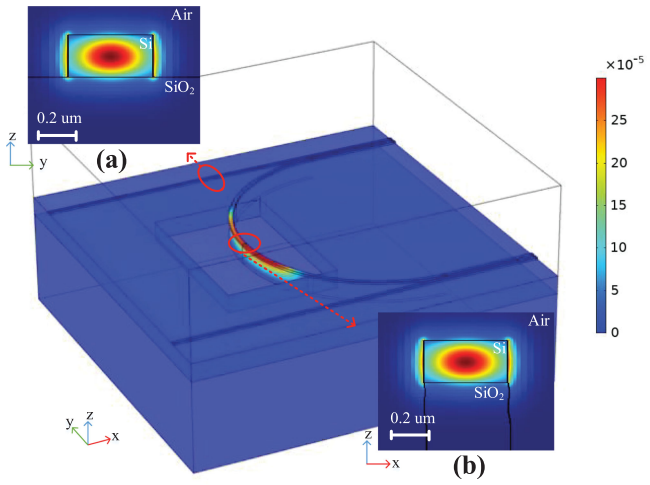

Fig. 2. Simulated deformation profile of the proposed senor. Inset: Fundamental mode profile of (a) normal straight silicon waveguide without etching, (b) silicon waveguide with surrounding oxide layer etched.

strain-induced resonance shift of the non-etched SOI microring is much smaller than the etched one [22]. To obtain a sensitive ultrasound receiver, the strain-induced deformation which is related to the parameter, $L_0(1+\epsilon(t))$, can be enhanced by etching away the silicon dioxide around the silicon waveguides via wet chemical etching or dry etching techniques based on plasma or reactive ion [23], which will enlarge the deformation of the microring resonator circumference. Since the coupling regions of the add-drop microring structure are intentionally preserved unetched and also located far away from the etched arc part, the coupling coefficients, r and k in Eq. (3) and Eq. (4), remains as constant under ultrasound pressure. Thus the transfer function measurement is free from distortions arising from deformations in the coupling region. We use the DSP unit to process the measured photocurrent at two ports of the proposed sensor in the time domain. Following by the calculation of photocurrent ratio, fast Fourier transform is also applied in the DSP unit as indicated in Fig. 1(b). Based on the sampling rate of analog-to-digital converter (ADC), the incoming unknown ultrasound signal is identified via mapping sampling number to the exact frequency.

As a proof-of-concept, we fabricated a racetrack ring resonator with a bending radius of 15 μm on a standard SOI wafer in the $\langle 1\ 0\ 0\rangle$ crystalline direction. It is noted that SOI waveguides guided in other orientation, such as $\langle 1\ 1\ 0\rangle$ crystalline direction, is also suitable for ultrasound measurement applications [20]. The waveguides of the resonator are 220 nm high and 450 nm wide, the buried oxide layer is 2 μm in height sitting on a 750 μm thick silicon substrate, and a 200 μm^2 (10 μm width by 20 μm length) oxide layer around the arc part of the silicon waveguide is etched away to enhance the ultrasound sensitivity as shown in Fig. 2. The light field propagation in the etched microring waveguide is then investigated through simulations including the acoustic-solid interaction and numerical mode analysis via COMSOL Multiphysics and Lumerical Finite Difference Eigenmode (FDE) solver respectively. Fig. 2 shows the simulation results when the ultrasound pressure is uniformly applied from the top surface. It can be seen from the gradual colour change that the etched arc part has greater deformation than waveguide close to silicon dioxide material while the coupling regions that are unetched remain unchanged under the same ultrasound pressure. Further, the calculated mode field profiles of the etched arc waveguide and the unetched bus waveguides are studied, and the results are shown in the inset (a) and the inset (b) in Fig. 2 respectively. The light is mostly confined inside the silicon core, which has larger refractive index than air or oxide cladding. The overlap percentage between the two mode profiles is over 99.92%, indicating a negligible mode conversion loss induced by the etching process. The simulation results, therefore, prove that

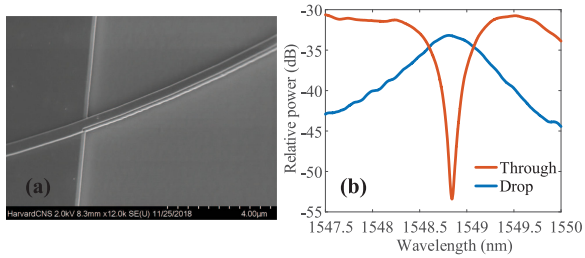

Fig. 3. (a) Scanning Electron Microscope (SEM) image of the deep-etched microring resonator. (b) Spectrum of the through and drop port of the fabricated microring resonator.

the proposed etching process can effectively enhance the ultrasound sensitivity of the microring without interfering with the coupling regions or inducing extra transmission losses.

3. Experimental Results and Discussion

A proof-of-concept experiment was carried out based on the schematic diagram shown in Fig. 1(a). The ultrasound sensor is constructed by using a racetrack resonator coupled with two bus waveguides in an SOI platform. The 450 nm by 220 nm silicon waveguides ensure the single mode transverse-electric field light propagation. There is a gap of 273 nm between the straight waveguide and the racetrack waveguide for evanescent coupling. Silicon waveguides in the arc part of the racetrack are deep-etched, where the side silicon oxide is etched away to enhance the sensor's sensitivity to the surrounding ultrasound vibration as shown in Fig. 3(a). The optical characteristics of the microring resonator were first measured without any ultrasound signal applied, where the spectrum of the microring resonator is shown in Fig. 3(b). In order to detect the ultrasound signal, a laser (Keysight 81960 A) with its wavelength fixed at 1548.9 nm was used to inject light into the sensor chip. The ultrasound signal was generated by using a ceramic transducer where the sinusoidal waves at ultrasonic frequencies were driven by an electrical function generator. Both through and drop ports of the sensing ring were monitored by a multiport optical power meter (Keysight N7744 A) for achieving high sensitivity and fast data processing. When the ultrasound was applied to the selectively-etched microring resonator, the optical power meter continuously logged the output powers from the drop and through ports. Since each input port of the optical power meter was controlled by the same inner clock, the data transmission discrepancy of both ports can be negligible. This ensures the synchronous measurement of the strain-induced variations of the photocurrents at the two ports of the add-drop microring resonator so that the transfer function can be accurately measured.

First, we investigate the sensing performance of the proposed integrated optical sensor on detecting ultrasound signals generated from an air-coupled transducer. Fig. 4(a) presents the measured transfer function of the sensor under a continuous air-coupled ultrasound wave at 58 kHz, while Fig. 4(b) provides the zoom-in view which exhibits a continuous sinusoidal-like waveform and a time period of about 17.23 μs. The frequency spectrum of the detected ultrasound signal via FFT is displayed in Fig. 4(c), it shows the sensor has a high Signal-to-noise ratio (SNR) of over 50 dB at the measured frequency. The high purity and no spurs in the frequency spectrum proves the linear response of the proposed sensor to the ultrasound signal.

To investigate the sensing resolution, ultrasound signals at closely placed frequencies were applied to the sensor. Fig. 5 shows the shift of the FFT spectrum when an ultrasound frequency change of 30 Hz was introduced, showing that the proposed sensor system is able to distinguish small frequency difference, which makes it applicable in a spectrally cluttered environment where precise frequency measurement for the incoming ultrasound wave is required. It is noted that the proposed sensor is also applicable for the detection of wideband acoustic signals. In practice, the sensor bandwidth can be improved by increasing the sampling rate of the DSP unit.

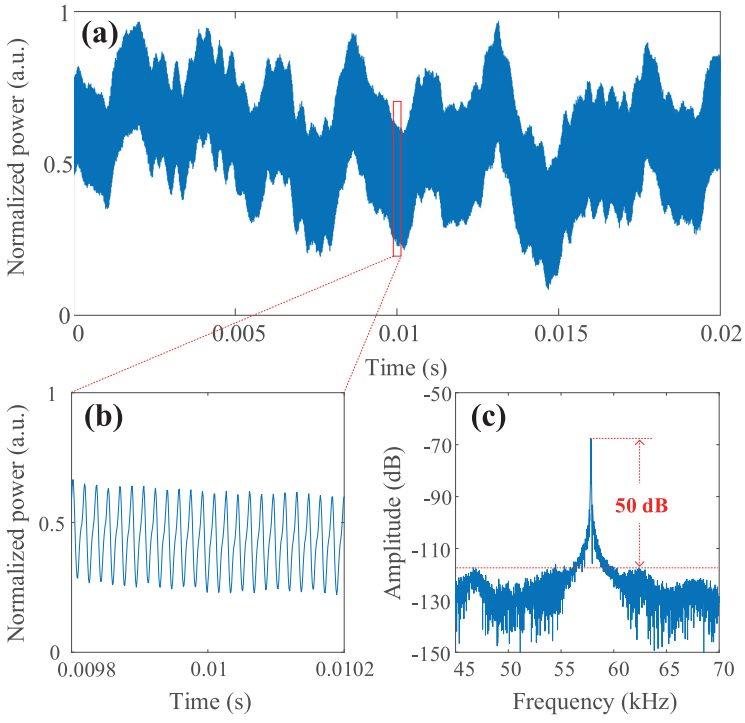

Fig. 4. (a) Measured transfer function of the microring resonator sensor to a 58 kHz air coupled ultrasound transducer. (b) Zoomed-in figure of the temporal signals for the sensor. (c) FFT spectrum of the temporal response.

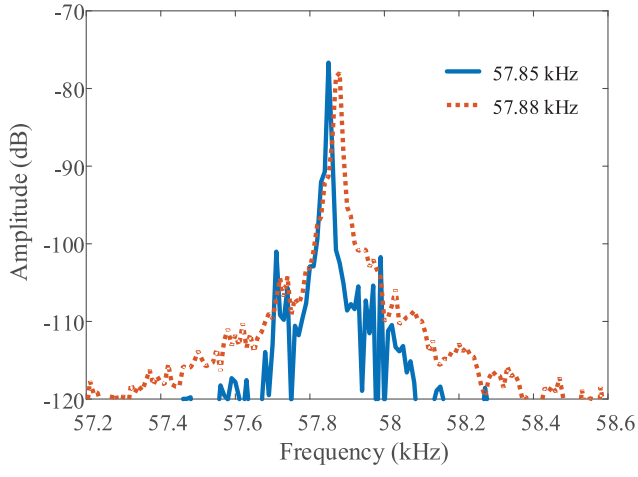

Fig. 5. The FFT spectrum response of the sensor for two closely spaced ultrasound inputs.

To investigate the sensing sensitivity, ultrasound signals with various sound pressure level (SPL) at 58 kHz were applied to the sensor. Fig. 6 illustrates the measured results showing the amplitude of the detected signal decreases correspondingly as the applied pressure drops from 42 Pa (126 dB SPL) to 4 Pa (106 dB SPL). The measurement was taken at the same ultrasound frequency (58 kHz), where offset frequencies were applied to distinguish different measurements. Note the detected signal of the sensor demonstrates a high SNR even at the 4 Pa pressure level indicating an excellent pressure sensitivity. We also varied the ultrasound frequencies between

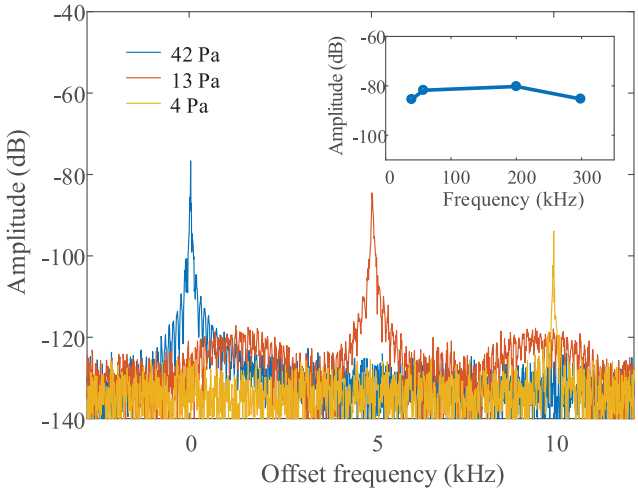

Fig. 6. Measured sensor response at difference pressure levels. Inset: Sensor response for different frequencies.

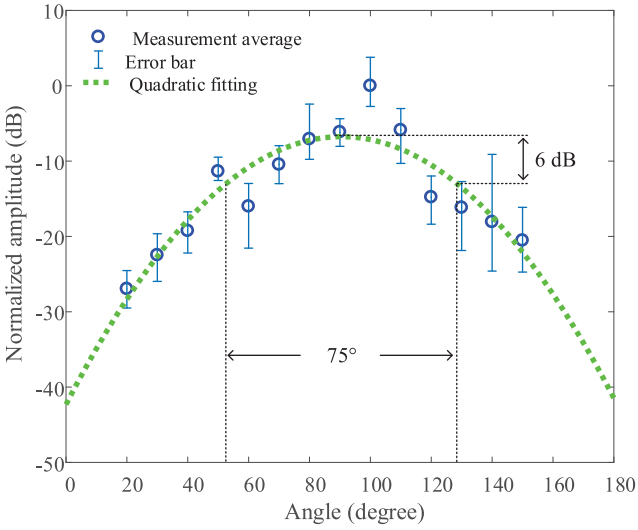

Fig. 7. Normalized angular response obtained by Fourier transfer of the temporal response from the proposed sensor.

40 to 300 kHz while maintaining the pressure level at around 126 SPL for the continuous waves. The result is shown in the inset of Fig. 6 demonstrating the wide frequency performance of the proposed microring resonator sensor. Here we investigated the sensor responses to ultrasound signals up to 300 kHz, which is a frequency range that can be utilized in structure health monitoring and photoacoustic imaging [24], [25]. Higher bandwidth measurement can be achieved by adding ultrasound absorbing media such as aqueous solution or making adjustments to the etching area and microring size with the consideration of the trade-off between bandwidth and sensitivity.

The ultrasound acceptance angle of the sensor is also investigated. Here the acceptance angle is defined as the angle formed by the axis on which the ultrasound wave is detected with 6 dB attenuation with respect to the signal detected right above the sensor center [26]. The ultrasound transducer working at 300 kHz was moved along a semicircle trajectory at a radius of 10 mm above the sensor in the vertical plane along the x axis shown in Fig. 2, where 90 degree is the angle when

the ultrasound transducer is placed right above the center of the microring resonator sensor probe. We took five continuous measurements at each angle from 20 degrees to 150 degrees range with a step of 10 degrees. The measured angle-dependent response is shown in Fig. 7. The average values are plotted as circle points and the vertical bar indicates the measurement errors which are mainly caused by the ambient variation of the experimental setup. The dash line shows the quadratic fitting of the measurement average points. The results show the fabricated sensor has the capacity to detect the ultrasound waves from an acceptance angle of 75 degrees.

4. Conclusion

In this work, we have successfully demonstrated a novel chip scale optical ultrasound sensor based on SOI platform. We derived the theoretical model, simulated the ultrasound sensing response and obtained a linear and consistent sensing response free from distortions arising from coupling region deformations. The proposed integrated optical sensor removes variations from the power fluctuation of the optical source and successfully detects ultrasound signals at different frequencies and magnitudes, and has a wide ultrasound receiving angle. Moreover, the compatibility and the potential of monolithic integration of the proposed sensor opens opportunities for various ultrasound sensing applications.

Acknowledgment

The authors would like to thank valuable discussions with Dr. J. Deng and Prof. M. Loncar from Harvard University and Dr. S. Chew from the University of Sydney. This fabrication was carried out at the Harvard Center for Nanoscale Systems (CNS), a member of the National Nanotechnology Infrastructure Network (NNIN).

References

[1] G. Wild and S. Hinckley, "Acousto-ultrasonic optical fiber sensors: Overview and state-of-the-art," *IEEE Sensors J.*, vol. 8, no. 7, pp. 1184–1193, Jul. 2008.
[2] Y. Xu, L. Zhang, S. Gao, P. Lu, S. Mihailov, and X. Bao, "Highly sensitive fiber random-grating-based random laser sensor for ultrasound detection," *Opt. Lett.*, vol. 42, no. 7, pp. 1353–1356, 2017.
[3] M. Xu and L. V. Wang, "Photoacoustic imaging in biomedicine," *Rev. Scientific Instrum.*, vol. 77, no. 4, 2006, Art. no. 041101.
[4] S. Basiri-Esfahani, A. Armin, S. Forstner, and W. P. Bowen, "Precision ultrasound sensing on a chip," *Nature Commun.*, vol. 10, no. 1, pp. 1–9, 2019.
[5] A. Rosenthal, D. Razansky, and V. Ntziachristos, "High-sensitivity compact ultrasonic detector based on a pi-phase-shifted fiber bragg grating," *Opt. Lett.*, vol. 36, no. 10, pp. 1833–1835, 2011.
[6] S.-W. Huang *et al.*, "Low-noise wideband ultrasound detection using polymer microring resonators," *Appl. Phys. Lett.*, vol. 92, no. 19, 2008, Art. no. 193509.
[7] B. Culshaw, G. Thursby, D. Betz, and B. Sorazu, "The detection of ultrasound using fiber-optic sensors," *IEEE Sensors J.*, vol. 8, no. 7, pp. 1360–1367, Jul. 2008.
[8] H. Tsuda, "Ultrasound and damage detection in CFRP using fiber bragg grating sensors," *Composites Sci. Technol.*, vol. 66, no. 5, pp. 676–683, 2006.
[9] H. Tsuda *et al.*, "Acoustic emission measurement using a strain-insensitive fiber bragg grating sensor under varying load conditions," *Opt. Lett.*, vol. 34, no. 19, pp. 2942–2944, 2009.
[10] W. Zhang *et al.*, "An optical fiber Fabry-Perot interferometric sensor based on functionalized diaphragm for ultrasound detection and imaging," *IEEE Photon. J.*, vol. 9, no. 3, Jun. 2017, Art. no. 16871039.
[11] B. Ouyang, Y. Li, M. Kruidhof, R. Horsten, K. W. Van Dongen, and J. Caro, "On-chip silicon machzehnder interferometer sensor for ultrasound detection," *Opt. Lett.*, vol. 44, no. 8, pp. 1928–1931, 2019.
[12] C. Zhang, S.-L. Chen, T. Ling, and L. J. Guo, "Review of imprinted polymer microrings as ultrasound detectors: Design, fabrication, and characterization," *IEEE Sensors J.*, vol. 15, no. 6, pp. 3241–3248, Jun. 2015.
[13] C.-Y. Chao, S. Ashkenazi, S.-W. Huang, M. O'Donnell, and L. J. Guo, "High-frequency ultrasound sensors using polymer microring resonators," *IEEE Trans. Ultrason., Ferroelect., Freq. Control*, vol. 54, no. 5, pp. 957–965, May 2007.
[14] S. Leinders *et al.*, "A sensitive optical micro-machined ultrasound sensor (OMUS) based on a silicon photonic ring resonator on an acoustical membrane," *Scientific Rep.*, vol. 5, 2015, Art. no. 14328.
[15] F. G. Peternella, B. Ouyang, R. Horsten, M. Haverdings, P. Kat, and J. Caro, "Interrogation of a ring-resonator ultrasound sensor using a fiber mach-zehnder interferometer," *Opt. Express*, vol. 25, no. 25, pp. 31 622–31 639, 2017.

[16] S. Zhang, J. Chen, and S. He, "Novel ultrasound detector based on small slot micro-ring resonator with ultrahigh q factor," *Opt. Commun.*, vol. 382, pp. 113–118, 2017.
[17] C. Zhang and C. Zhao, "Sensitive label-free and compact ultrasonic sensor based on double silicon-on-insulator slot micro-ring resonators," *Optik*, vol. 178, pp. 1029–1034, 2019.
[18] A. L. Lopez-Sanchez and L. W. Schmerr, "Determination of an ultrasonic transducer's sensitivity and impedance in a pulse-echo setup," *IEEE Trans. Ultrason., Ferroelect., Freq. Control*, vol. 53, no. 11, pp. 2101–2112, Nov. 2006.
[19] W. J. Westerveld *et al.*, "Characterization of a photonic strain sensor in silicon-on-insulator technology," *Opt. Lett.*, vol. 37, no. 4, pp. 479–481, 2012.
[20] W. J. Westerveld *et al.*, "Characterization of integrated optical strain sensors based on silicon waveguides," *IEEE J. Sel. Topics Quantum Electron.*, vol. 20, no. 4, pp. 1–10, Jul./Aug. 2014.
[21] W. Bogaerts *et al.*, "Silicon-on-insulator spectral filters fabricated with CMOS technology," *IEEE J. Sel. Topics Quantum Electron.*, vol. 16, no. 1, pp. 33–44, Jan./Feb. 2010.
[22] E. Hallynck and P. Bienstman, "Integrated optical pressure sensors in silicon-on-insulator," *IEEE Photon. J.*, vol. 4, no. 2, Apr. 2012, Art. no. 12637633.
[23] Y. Nishi and R. Doering, *Handbook of Semiconductor Manufacturing Technology*. Boca Raton, FL, USA: CRC Press, 2007.
[24] K. H. Kim *et al.*, "Air-coupled ultrasound detection using capillary-based optical ring resonators," *Sci. Rep.*, vol. 7, no. 1, pp. 1–11, 2017.
[25] F. Amerini and M. Meo, "Structural health monitoring of bolted joints using linear and nonlinear acoustic/ultrasound methods," *Structural Health Monit.*, vol. 10, no. 6, pp. 659–672, 2011.
[26] G. Wissmeyer, M. A. Pleitez, A. Rosenthal, and V. Ntziachristos, "Looking at sound: Optoacoustics with all-optical ultrasound detection," *Light Sci. Appl.*, vol. 7, no. 1, pp. 1–16, 2018.